Journal of Biomedical Optics

SPIEDigitalLibrary.org/jbo

Effect of polyethylene glycol coatings on uptake of indocyanine green loaded nanocapsules by human spleen macrophages *in vitro*

Baharak Bahmani
Sharad Gupta
Srigokul Upadhyayula
Valentine I. Vullev
Bahman Anvari

SPIE

Effect of polyethylene glycol coatings on uptake of indocyanine green loaded nanocapsules by human spleen macrophages *in vitro*

Baharak Bahmani,[a] Sharad Gupta,[a] Srigokul Upadhyayula,[b] Valentine I. Vullev,[a,b] and Bahman Anvari[a]
[a]University of California, Riverside, Department of Bioengineering, Riverside, California 92521
[b]University of California, Riverside, Department of Biochemistry and Molecular Biology, Riverside, California 92521

Abstract. Near-infrared (NIR) optically active nanoparticles are promising exogenous chromophores for applications in medical imaging and phototherapy. Since nanoparticles can be rapidly eliminated from the body by cells of the reticuloendothelial system, a thriving strategy to increase their blood circulation time is through surface modification with polyethylene glycol (PEG). We constructed polymeric nanocapsules loaded with indocyanine green (ICG), an FDA-approved NIR dye, and coated with aldehyde-terminated PEG. Using optical absorbance spectroscopy and flow cytometry, we investigated the effect of PEG coating and molecular weight (MW) of PEG [5000 and 30,000 Daltons (Da)] on the phagocytic content of human spleen macrophages incubated with ICG-containing nanocapsules (ICG-NCs) between 15 to 360 min. Our results indicate that surface coating with PEG is an effective method to reduce the phagocytic content of ICG-NCs within macrophages for at least up to 360 min of incubation time. Coating the surface of ICG-NCs with the low MW PEG results in lower phagocytic content of ICG-NCs within macrophages for at least up to 60 min of incubation time as compared to ICG-NCs coated with the high MW PEG. Surface coating of ICG-NCs with PEG is a promising approach to prolong vasculature circulation time of ICG for NIR imaging and phototherapeutic applications. [DOI: 10.1117/1.3574761]

Keywords: Fluorescent probe; laser therapy; nanomedicine; optical imaging; phagocytic cells.

Paper 10558SSR received Oct. 14, 2010; revised manuscript received Jan. 11, 2011; accepted for publication Jan. 12, 2011; published online May 10, 2011.

1 Introduction

The ability to detect and visualize tissue and vascular malformations constitutes a fundamentally crucial step for early diagnosis of disease, selecting an appropriate therapeutic approach, and monitoring the effectiveness of the therapy. For example, early and accurate tumor detection is the first step toward diagnosis, treatment, and clinical management of cancer. Development of highly sensitive probes with high specificity that would enable diagnosis of pre-malignant lesions and early stage tumors remains as one of the great challenges of oncology. Recent advances in extreme miniaturization to the nanoscale now provide the technological basis and potential for the development of nanosized materials that may enable early diagnosis and treatment of a wide range of diseases such as cancer at cellular and molecular levels. In recent years, such nanomaterials have been studied for their utilities in imaging of tissue abnormalities, including cancerous cells, and delivering therapeutic drugs.[1–4]

Near-infrared (NIR) fluorescence imaging using exogenous chromophores with sizes on the nano-scale has been gaining increased attention as an enabling technology with highly sensitive and target specific capabilities.[4–10] The use of NIR wavelengths is particularly advantageous, in that there is relatively deep optical penetration and emission (on the order of several centimeters) over this spectral bandwidth with minimal autofluorescence. Additionally, utilization of NIR wavelengths in combination with nanoscale optical contrast agents can provide a methodology for subcellular and molecular imaging.

Indocyanine green (ICG) is a cyanine NIR dye approved by United States Food and Drug Administration (FDA) for assessment of cardiac output, hepatic function, and ophthalmological vascular imaging.[11–15] Additionally, ICG has been studied for potential phototherapeutic applications including photothermal destruction of tumors and photocoagulation of blood vessels,[16–18] treatment of skin disorders,[19–21] and as a sensitizer for photodynamic therapy of cancer.[22,23]

The current method of administering ICG is by dissolving it in isotonic saline solution and intravenously delivering it. Despite its clinical usage, ICG in its current formulation, suffers from several major drawbacks: 1. concentration of the ICG solution and the nature of the solvent have a significant influence on its absorption properties;[24–27] 2. after a bolus injection, ICG readily binds to albumin and high-density lipoproteins in blood plasma, resulting in changes in its optical absorbance and fluorescence emission properties;[28,29] and 3. ICG is rapidly cleared from the body, showing a rapid vascular clearance with half-life on the order of 3 to 4 min,[30,31] and eliminated from the general circulation by hepatocytes.

Given the optical instability of ICG when exposed to physiologically relevant conditions (e.g., blood plasma and body temperature), its short vascular circulation time, and nearly

Address all correspondence to: Bahman Anvari, University of California, Riverside, Department of Bioengineering, Riverside, California 92521. Tel.: 951-827-5726; Fax: 951-827-6414; E-mail: anvarib@ucr.edu.

1083-3668/2011/16(5)/051303/10/$25.00 © 2011 SPIE

exclusive uptake by the liver, the true potential of this nontoxic and clinically proven exogenous chromophore for optical imaging and phototherapeutic applications remains limited. Recent studies demonstrate that encapsulation of organic dyes help stabilize their optical properties, mainly due to the protecting role of the encapsulating structure, which shields the embedded fluorophore from the external environment.[32,33] To-date, a number of nanoconstructs have been developed to encapsulate ICG. These systems have been constructed from polymeric micelles formed from poly(styrene-alt-maleic anhydride)-block-poly(styrene) diblock copolymers,[34] polylactic co(glycolic)-acid (PLGA) particle,[33,35] phospholipid emulsions,[36,37] modified silicate matrices,[38] and calcium phosphate.[9] These studies have demonstrated improved optical stability of ICG resulting from encapsulation and are very encouraging in that they demonstrate nano-encapsulation of ICG provides a potential technique for targeted optical imaging.

We have previously reported on ICG loading into polymeric nanocapsules composed of cross-linked poly(allylamine) hydrochloride (PAH) and sodium salt.[32,39–43] Certain advantages, associated with our ICG-containing nanocapsules (ICG-NCs), set them apart from other ICG-doped constructs. Our constructs are spontaneously self-assembled via green-chemistry in aqueous media within 10 to 30 s, and the total time to impregnate the nanocapsules with ICG does not exceed two hours. The self-assembly of a readily available polymer (PAH) via electrostatically-driven cross-linking with multivalent inorganic anions, phosphates, produces capsules with a broad range of sizes and physical stability with ability for different types of dye loading.

A common problem that nearly all types of nanoparticles will have to overcome once within the vasculature is the issue of clearance from the vasculature and nonspecific recognition. Cells of the reticuloendothelial system (RES), comprised of liver, spleen, and bone marrow, play a key role in the clearance of foreign particles from circulation. The interaction between these cells and nanoparticles is mediated through the presence of specific proteins adsorbed on the surface of nanoparticles. *In-vivo* clearance of nanoparticles from circulation is dependent on the level of protein adsorption on their surface and intracellular uptake by the cells of RES.[44–47] Therefore, shielding the nanoparticles from macrophages of RES, by minimizing the interaction between macrophages receptors and proteins adsorbed on the surface of nanoparticles, is expected to increase the circulation time of the nanoparticles.

Use of polyethylene glycol (PEG) to coat the surface of nanoparticles has been investigated as a methodology to minimize the interaction between nanoparticles and macrophages.[48–54] PEG is a water-soluble biocompatible polymer with highly ambulant and flexible chains.[55] On a PEGylated surface, the major forces between the surface and proteins in the solution are steric repulsion, van der Waals attraction and hydrophobic interaction.[56] When the steric repulsion prevails the attraction forces between proteins and PEG chains, the surface becomes less susceptible to protein adsorption.[57–59]

The density and conformation of PEG molecules on the surface are two crucial factors in determining the net interfacial forces governing protein adsorption. On a low-density PEGylated surface, the steric repulsion force between the proteins attempting to attach to such surface would be smaller as a result of reduced hydration energy per chain and unit surface. The conformation of PEG chains on the surface depends on the molecular weight (MW) of the PEG. In low MW PEG, chains extend out in helical conformation and form a brush-like layer. However, in high MW PEG, chains entangle with each other and form a mushroom-like layer.[60–65]

As the first step toward characterizing the influence of PEGylating the surface of ICG-NCs on circulation and biodistribution of the capsules, herein, we report the effects of ICG-NCs surface PEGylation on the uptake of the capsules by human spleen macrophages *in vitro*. Specifically, we investigate the effect of PEG's MW on the uptake level of the ICG-NCs by macrophages. The results presented here provide a basis for the design of ICG-NCs with optimal surface properties required for prolonged circulation of these nanocapsules *in vivo*.

2 Materials and Methods

2.1 *Materials*

Sodium phosphate dibasic heptahydrate ($Na_2HPO_4.7H_2O$, Fisher Scientific), poly(allylamine) hydrochloride (PAH, Sigma-Aldrich), indocyanine green (Sigma-Aldrich), methoxy-poly (ethylene glycol)-butyraldehyde (PEG-ALD, MW = 5000 and 30,000 Da, Laysan Bio Inc.), Sodium dithionite ($Na_2S_2O_4$, Sigma-Aldrich), and phosphate buffer saline (PBS, Fisher BioReagents) were used as purchased. Human spleen macrophages (KMA cell line) were purchased from American Type Culture Collection (ATCC®). Cells were cultured in Iscove's modified Dulbecco's medium (IMDM) supplemented with 4 mM L-glutamine, 1.5 g/L sodium bicarbonate, 0.02 mM thymidine, 0.1 mM hypoxanthine, 0.05 mM 2-mercaptoethanol, 10% fetal bovine serum, and 1% penicillin.

2.2 *Synthesis of ICG-loaded Nanocapsules*

ICG-NCs were synthesized through a self-assembly method previously described in detail.[32,39–43] First, a polymeric aggregate was formed through ionic cross-linking between 20 μL of PAH solution (2 mg/mL DI water, 4°C) and 60 μL of disodium phosphate salt solution (0.01 M in DI water, 4°C) by mixing them for 10 s. Subsequently, 1.2 mL of cooled de-ionized water (4°C) was added to the polymeric aggregate suspension, immediately followed by the addition of 240 μL of cooled ICG stock solution (500 μg/mL DI water, 4°C). The nanocapsule suspension was mixed for 10 s and then aged for 20 min in darkness at 4°C. The nanocapsule suspension was washed twice through centrifugation at 3000 rpm for 2 h at 4°C.

The size of the polymeric aggregate formed during the first step of synthesis can be tuned by altering the ratio of total negative charge of the Na_2HPO_4 salt to the total positive charge of PAH, defined as R ratio.[39,43] In this study, R value was set at 2. Using an R ratio higher than 2 will result in the formation of larger and fast growing aggregates.

2.3 *PEG-coating*

After ICG-NCs were formed, the amine groups on the surface of the capsules were used as the sites for covalent coupling

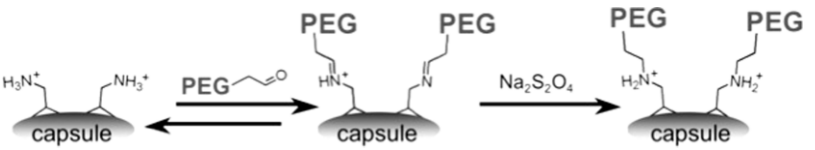

Fig. 1 Synthesis procedure for PEGylation of ICG-loaded nanocapsules through reductive amination.

with aldehyde-terminated polyethylene glycol (PEG-ALD) via reductive amination. Reductive amination is an important technique to form a covalent bond between carbon and nitrogen.[66] In this process, an aldehyde or ketone is condensed with an amine in the presence of a reducing agent. Since hydride reducing agents, such as cyanoborohydride, are detrimental for cyanine dyes, we employed sodium dithionite, as a reductant in coating the ICG-NCs. The Schiff base (i.e., the imine) formed between the aldehyde-terminated PEGs and the surface amines of the nanocapsules is not sufficiently stable under physiological conditions. Therefore, we added sodium dithionite, to irreversibly convert the imines into amines and afford covalent coating of the nanocapsules with PEG (Fig. 1).

Since a maximum of three PEG chains can be conjugated on $\approx$1 nm^2, we aimed to achieve a minimum number density of 1 chain/nm^2 by conjugating at least 10 aldehyde-terminated PEG chains per 10 nm^2 of nanocapsule surface, and determined the required amount of PEG-ALD based on diameter and number of nanocapsules in the suspension.

Aldehyde-terminated PEGs with two different MWs (5000 Da and 30000 Da) were used. Sodium dithionite added as a solid to the nanocapsules suspension at approximately two equivalents per mole PEG-ALD. The suspension of ICG-NCs, PEG-ALD and Sodium dithionite was aged for at least 8 h in darkness at 4°C. The sample was then dialyzed in water for 48 h in darkness at 4°C. Water was changed every 12 h during the dialysis. To separate any possible remaining reducing agent, the sample was centrifuged at 3000 rpm for 2 h (twice) at 4°C. As a control set, ICG-NCs were noncovalently coated with PEG-ALD in the absence of the reducing agent, resulting in the formation of an unstable Schiff base between amine groups on the surface of ICG-NCs and the PEG-ALD molecules.

2.4 *Characterization of Nanocapsules*

The morphology of lyophilized uncoated ICG-NCs was examined by scanning electron microscopy (SEM, Philips, XL-30 FEG). Diameter distribution of these capsules was quantified by analysis of the SEM images using the ImageJ software.

Optical absorption spectra of PEG-coated ICG-NCs were obtained using a UV-Visible spectrophotometer (Cary 50 UV-Vis spectrophotometer). Fluorescence spectra of free ICG and ICG-NCs were obtained with a fluorometer (Jobin-Yvon Fluorolog) in response to 680 nm excitation wavelength.

Presence of PEG on the surface of nanocapsules was verified by Fourier transform infrared spectroscopy (FTIR) using a Perkin-Elmer 1600 series spectrometer. The zeta (ζ)-potentials of nanocapsules were measured by laser Doppler Velocimetry (Zetasizer Nanoseries, Nano-ZS90) to further confirm PEGylation.

2.5 *Incubation of Human Spleen Macrophages with ICG-NCs for Fluorescent Imaging*

To study the interaction of ICG-NCs with cells of RES, ICG-NCs were incubated with human spleen macrophages. We added 200 μl of cell suspension ($\approx 5 \times 10^5$ cells/ml) in growth media (IMDM) to each well of a 96-well flat-bottomed micro-titer plate. Subsequently, 100 μl of uncoated ICG-NCs, PEG-ALD (MW = 5000 Da) coated ICG-loaded nanocapsules (PEG-5k-coated ICG-NCs), and PEG-ALD (MW = 30000 Da) coated ICG-loaded nanocapsules (PEG-30k-coated ICG-NCs) were separately added to cell suspensions. Freely dissolved ICG (free ICG) in PBS was used as positive control and cell suspension without ICG-NCs or free ICG was considered as negative control.

Cells were incubated with samples and positive control for 30 min and 2 h without exposure to light in an incubator at 37°C with 5% CO_2. Following incubation, the suspension of cells and ICG-NCs were washed at low-speed centrifugation (1200 rpm) to separate any remaining suspended NCs from cells.

2.6 *Fluorescent Imaging of Spleen Macrophages*

Cells were resuspended in growth medium after centrifugation. An electron multiplier (EM) gained CCD camera (Quant EM-CCD, Hamamatsu) in combination with a long pass emission filter (>770 nm) were used to capture the fluorescent images of the cells in response to 740 $\pm$ 35 nm excitation wavelength. Camera exposure time was set at 0.1 s in all imaging sessions. The contrast and brightness window of all fluorescent images were normalized to the fluorescent image of cells incubated with free ICG (positive control) using ImageJ software.

2.7 *Quantification of ICG Content within Macrophages*

Following incubation with ICG-NCs or free ICG, macrophages were dissolved in sodium dedecyl sulfate (SDS). Upon exposure to SDS, macrophages are lysed and release their ICG content. The absorption spectra of solutions containing the lysed cells in SDS were collected. We took advantage of exclusive NIR absorbance by ICG to quantify the ICG content of lysed cells. Specifically, the ICG content was quantified using a calibration that yielded a linear relationship between peak absorbance at λ = 790 nm, and ICG dissolved in SDS at different concentrations. Saxena et al.[67] and Yaseen et al.[42] have used a similar method to quantify the uptake of ICG-containing PLGA nanoconstructs by cervical cancer cell lines *in vitro* and biodistribution of PAH-based ICG-NCs in healthy mice, respectively.

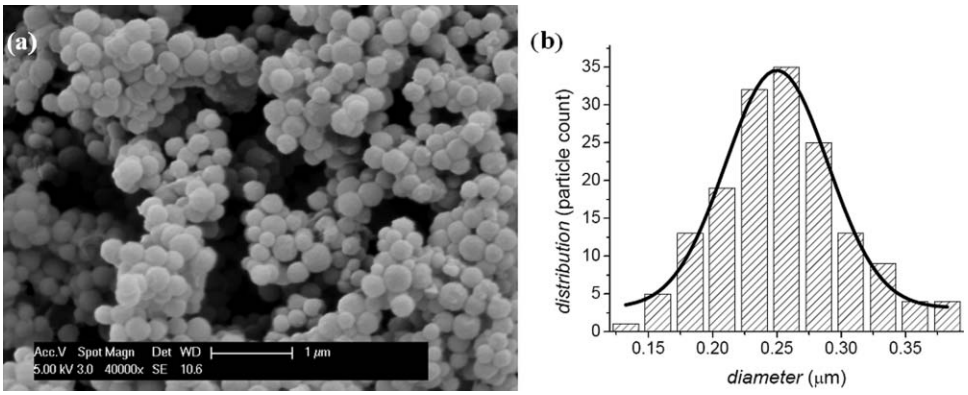

Fig. 2 (a) SEM image and (b) diameter distribution of lyophilized uncoated ICG-loaded nanocapsules. A Gaussian fit to the measured diameter distribution is also shown in panel (b).

2.8 *Characterization of ICG-NCs Phagocytic Content by Flow Cytometry*

We used flow cytometry to characterize the phagocytic content of ICG-NCs. Human spleen macrophages were incubated with free ICG, uncoated, and PEG-coated ICG-NCs for various time intervals ranging between 15 to 360 min. Following each incubation time, we detected the fluorescent emission from a large population of human spleen macrophages exposed to free ICG and ICG-NCs by flow cytometry. Cells were washed with PBS twice through centrifugation (1200 rpm for 4 min) and resuspended in PBS. Fluorescein isothiocyanate (FITC) Annexin V (BD Biosciences) apoptosis detection kit and propidium iodide (PI) were used to identify late apoptotic and dead cells, respectively, so that these cells would be excluded from the analysis. Macrophages were also labeled with fluorescent marker Phycoerythrin (PE) mouse anti-human CD11b/Mac-1. The integrin receptor CD11b/Mac-1 regulates the adherence and survival of activated macrophages. Therefore, we utilized the PE mouse anti-human CD11b/Mac-1 to discern activated macrophages from any other cell types. The prepared cells were analyzed by flow cytometer (BD FACSAria cell sorter) using 633 nm excitation and 785 nm emission wavelength for ICG detection. The fluorescent intensity distributions and mean fluorescent intensity (MFI) of PI negative but PE mouse anti-human CD11b/Mac-1 positive cells were used to quantify the interaction level of the human spleen macrophages with free ICG or ICG-NCs.

3 Results and Discussion

3.1 *Nanocapsules Characterization*

ICG-NCs were spherical in shape [Fig. 2(a)]. Diameter distribution of lyophilized uncoated ICG-NCs, as determined from the analysis of SEM images, is shown in Fig. 2(b). The particles mean diameter was 250 $\pm$ 40 nm.

The optical absorption and fluorescence spectra of free ICG, uncoated ICG-NCs, PEG-5k-coated ICG-NCs, and PEG-30k-coated ICG-NCs are shown in Fig. 3. Concentration of free ICG and that used to construct the ICG-NCs were 4 and 3 μM, respectively. The absorption spectrum for free ICG displays the peak absorbance values at 780 and 680 nm, corresponding to the monomeric and dimeric forms of ICG, respectively. Increased absorbance values in the spectral bands of 570 to 765 nm and $>$814 nm are observed for uncoated and PEG-coated ICG-NCs [Fig. 3(a)]. There are red shifts in the wavelengths associated with monomeric and dimeric forms for PEG-coated ICG-NCs. The difference in absorbance values are between 0 to 5% for uncoated and PEG-coated ICG-NCs in the 550 to 810 nm spectral range and virtually none for wavelengths greater than $\approx$810 nm

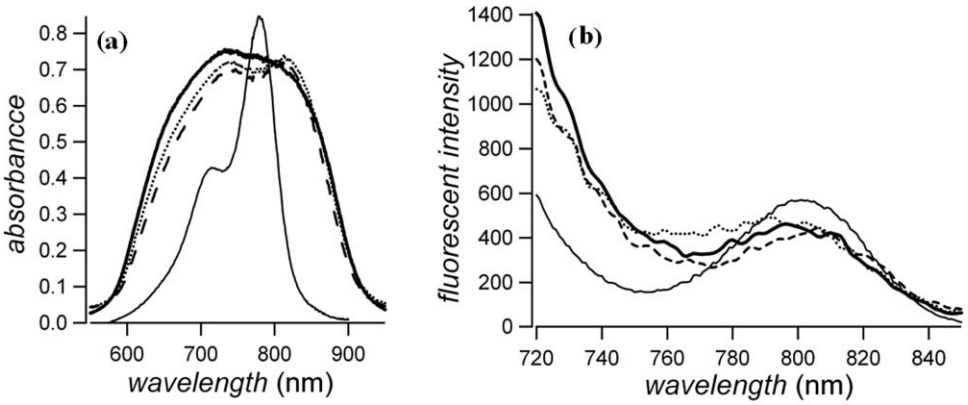

Fig. 3 (a) Absorption and (b) emission spectra of PEG-5k-coated ICG-NCs (dotted line), PEG-30k-coated ICG-NCs (dashed line), uncoated ICG-NCs (thin solid line), and freely dissolved ICG in water (thick solid line). The emission spectra of uncoated and PEG-coated ICG-NCs were smoothed using IGOR Pro software with second order binominal algorithm.

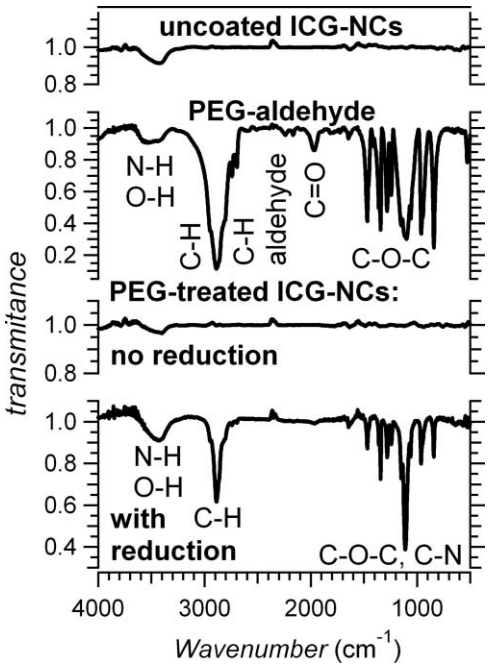

Fig. 4 FTIR spectra of uncoated ICG-NCs, PEG-aldehyde, and PEG-treated ICG-NCs with and without the reductive amination step.

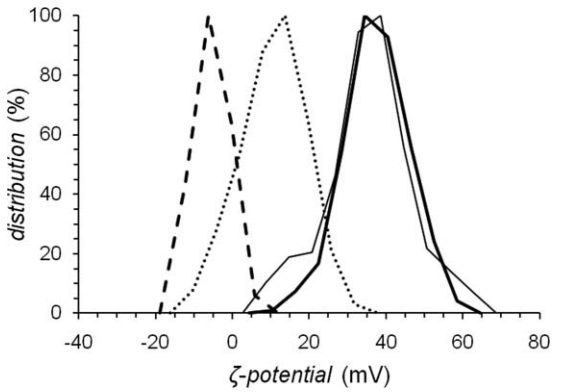

Fig. 5 ζ-potential distributions measured in water and at room temperature for various ICG-NCS: uncoated (thick solid line), PEG-30k-coated without reductive amination (thin solid line), PEG-5k-coated with reductive amination (dotted line), and PEG-30k-coated with reductive amination (dashed line).

[Fig. 3(a)]. There are very minimal differences in absorbance values of PEG-5k and PEG-30k coated ICG-NCs. Changes in absorption spectra of uncoated and PEG-coated ICG-NCs may be induced by conformational changes in ICG within the confined environment of the capsules and have also been reported in previous reports utilizing PAH-based ICG-NCs.[39,43]

The fluorescence spectra indicate that there is reduced emission in the narrow 720 to 730 nm band for PEGylated ICG-NCs [Fig. 3(b)]. Interestingly, over the 750 to 790 nm spectral band, there is increased emission from PEG-5k-coated ICG-NCs as compared to uncoated capsules. Overall, the spectra presented in Fig. 3 suggest that PEGylation does not compromise the absorbance and emission characteristics of ICG-NCs.

The characteristic peaks of PEG-ALD were observed in the FTIR spectra of ICG-NCs with the coating achieved by performing the reduction step (Fig. 4). The peak at $\sim$3500 cm^{-1} in both spectra for PEG-ALD and PEG-coated ICG-NCs is attributed to the N–H and O–H bonds. The sharp peak at $\sim$2900 cm^{-1} in these two spectra corresponds to C–H stretching. The peaks at $\sim$2650 to 2750 and $\sim$1900 cm^{-1} in the pure PEG-ALD spectrum are attributed to the aldehyde (O=)C–H stretch, and the carbonyl group (aldehyde C=O stretching), respectively, and both of these peaks are absent in the spectrum of PEG-treated ICG-NCs with reduction step. The peaks in the 900 to 1500 cm^{-1} range correspond to vibrational modes of C–O–C bonds of PEG in the spectra of pure PEG-ALD and PEG-coated ICG-NCs. The sharp peak at $\sim$1100 cm^{-1} in PEG-coated ICG-NCs spectra is vibrational mode of C–N bond. No specific peaks of PEG-ALD were detected for the PEG-treated ICG-NCs without the reduction step indicating the necessity to perform this step in order to achieve successful PEGylation. That spectrum was similar to that of uncoated ICG-NCs, indicating that amination coupling in the absence of the reducing agent did not yield PEG coatings on ICG-NCs.

The ζ-potential distribution (in -20 to $+50$ mV range) and its peak value ($\approx$40 mV) for uncoated ICG-NCs were nearly identical to those of the capsules where formation of PEG-ALD coating was attempted without the reduction step (Fig. 5). These similarities indicate that in the absence of the reduction step, PEG-ALD coating cannot be successfully produced. When utilizing the reductive amination step, the ζ-potential distributions for PEG-5k-coated ICG-NCs and PEG-30k-coated ICG-NCs were altered with the respective peak values shifted to $\approx$12 and -7 mV, indicating successful formation of PEG-ALD coating on the surface of the capsules. The reduction in ζ-potential of PEGylated samples could be due to the increase in thickness of a stern layer formed around the PEG-coated ICG-NCs. Subsequently, the position of the slipping plane at the electrical double layer will change and move away from the surface of ICG-NCs.[68–70]

3.2 *Fluorescence Imaging of Cells*

No or minimal fluorescence was detected from human spleen macrophages at 30 min and 2 h of incubation with PEG-5k-coated ICG-NCs and PEG-30k-coated ICG-NCs [Figs. 6(a)–6(d)]. The number of cells emitting fluorescence increased in response to incubation with uncoated ICG-NCs [Figs. 6(e) and 6(f)], with the highest number of cells and the most intense signal emanating from macrophages incubated with freely dissolved ICG [Figs. 6(g)–6(h)].

3.3 *Quantification of ICG Content within Macrophages*

In Fig. 7, we present results that display the ICG content of human spleen macrophages incubated with PEG-5k-coated ICG-NCs, PEG-30k-coated ICG-NCs, uncoated ICG-NCs, and free ICG for 30 min and 2 h. The highest ICG content was associated with macrophages incubated with free ICG for both incubation times. The content of PEG-5k-coated ICG-NCs by the human spleen macrophages was significantly lower than that of PEG-30k-coated (p-value

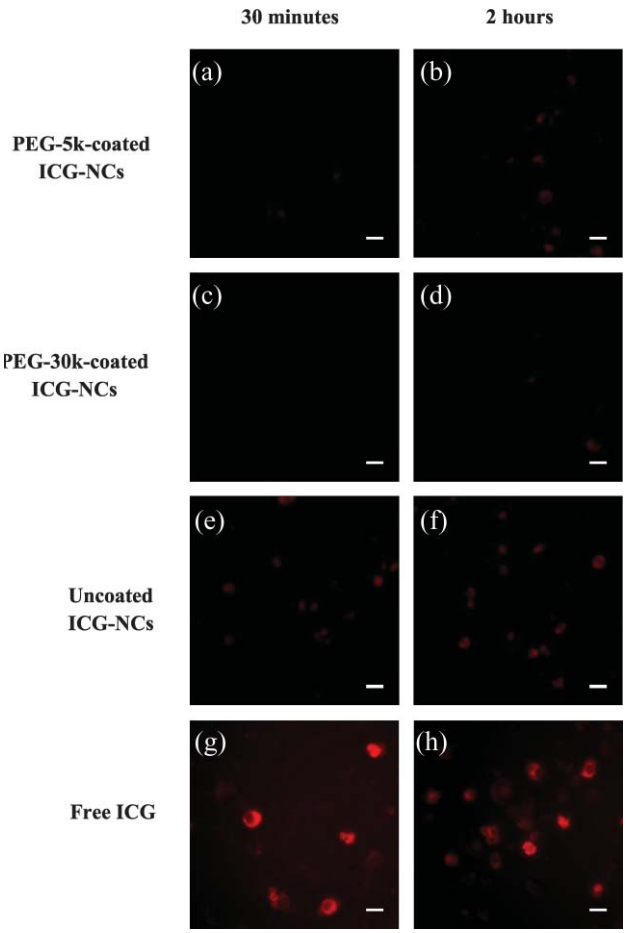

Fig. 6 Fluorescent images of human spleen macrophages incubated with: (a) and (b) PEG-5k-coated ICG-NCs; (c) and (d) PEG-30k-coated ICG-NCs; (e) and (f) uncoated ICG-NCs; and (g) and (h) freely dissolved ICG in PBS, for 30 min and 2 h, respectively.

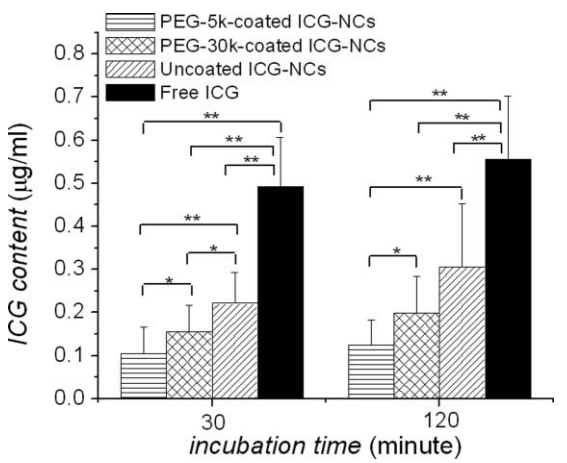

Fig. 7 Mean ICG content of human spleen macrophages incubated with PEG-5k-coated ICG-NCs, PEG-30k-coated ICG-NCs, uncoated ICG-NCs, and freely dissolved ICG in PBS for 30 and 120 min at 37°C (cell density = 5×10^5 cells/ml, $n = 7$). Error bars represent the standard deviation. Single and double asterisks statistically denote significance differences between the shown pairs with p-value < 0.05 and < 0.005, respectively.

< 0.05) and uncoated ICG-NCs (p-value < 0.005) for up to 120 min of incubation time. While, the content of PEG-30k-coated ICG-NCs was significantly higher than that of PEG-5k-coated ICG-NCs, it was still lower than uncoated ICG-NCs (p-value < 0.05).

3.4 *Characterization of ICG-NCs Phagocytic Content*

The population distribution of macrophages demonstrating various ICG fluorescent intensities after 15 min of incubation with free ICG or ICG-NCs, as determined by flow cytometry, are shown in Fig. 8(a). Macrophages incubated with free ICG exhibited the largest peak fluorescent value (≈1600). For macrophages incubated with uncoated, PEG-30k-coated, or PEG-5k-coated ICG-NCs, the respective peak fluorescent values became progressively lower. These results suggest that the use of PEG-5k as the coating material tends to minimize the phagocytic content of macrophages for short incubation times (15 min).

The MFI of macrophages incubated with free ICG and ICG-NCs between 15 to 360 min are shown in Fig. 8(b). For all incubation times, macrophages incubated with free ICG exhibited the highest MFI. Macrophages incubated with PEG-5k-coated ICG-NCs for up to 60 min had the lowest MFI values. Incubating the macrophages with PEG-coated ICG-NCs resulted in significantly lower MFI values for up to 360 min as compared to cells that were incubated with uncoated ICG-NCs. For incubation times of two hours and longer, there was no significant difference in MFI values for PEG-5k and PEG-30k-coated ICG-NCs.

The content of ICG-NCs within the macrophages at any time is the sum of the uptaken capsules that are still intact plus the capsules that are undergoing degradation (partially degraded) and fully degraded capsules. With increased incubation time, all of these fractions may be simultaneously present within the macrophages. As ICG or ICG-NCs become degraded, it is likely that their fluorescence characteristics change to give rise to a net reduced MFI. For incubation times up to 60 min, the intact ICG-NCs appear to be the dominant fraction since the MFI values for macrophages incubated with either uncoated or PEG-coated ICG-NCs monotonically increased during this time interval [Fig. 8(b)]. Beyond 60 min, the MFI values tend to fluctuate with incubation time, suggesting that all fraction types are likely to be present within the macrophages. Therefore, for long incubation times, the MFI will depend on the relative amount of each fraction type and its associated fluorescent emission characteristics.

The results of flow cytometry experiments [Fig. 8(b)] are consistent with those obtained by cell lysis followed by optical absorbance measurements (Fig. 7) with the exception of the phagocytic content of PEG-5k- and PEG-30k-coated ICG-NCs at two hours of incubation relative to each other. In the latter method, content quantification of ICG-NCs is based on the optical absorbance of ICG within the cell that includes the amount liberated from the intercellular phagocytic compartments after cell lysis. In flow cytometry studies, macrophages remain intact, and the measured MFI is related to the emission characteristics of internalized but not degraded ICG-NCs as wells as the degraded capsules and those undergoing degradation.

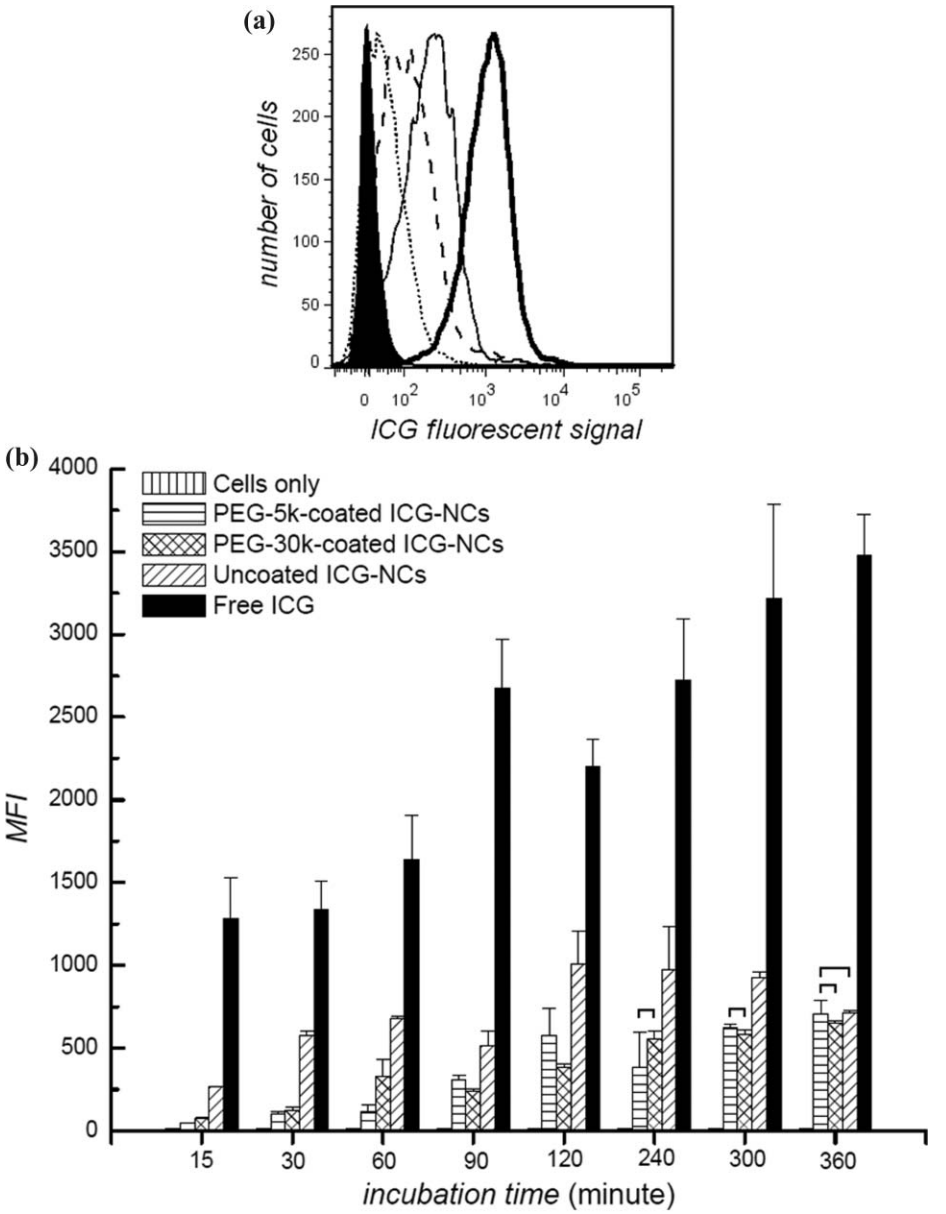

Fig. 8 Characterizing the phagocytic content of ICG-NCs within macrophages by flow cytometry. (a) Illustrative ICG fluorescent signals for populations of macrophages incubated with free ICG (thick solid line), uncoated ICG-NCs (thin solid line), PEG-5k-coated ICG-NCs (dotted line), or PEG-30k-coated ICG-NCs (dashed line) for 15 min. Macrophages not incubated with ICG or ICG-NCs were used as control (filled). (b) Mean fluorescent intensity (MFI) of macrophages (1×10^6 cells/well) after incubation with freely dissolved ICG, uncoated, PEG-5k-coated, and PEG-30k-coated ICG-NCs for various times ranging from 15 min to 6 h at 37°C. Experiments were repeated three times, and in each experiment, approximately 10,000 cells were examined. Each bar represents the MFI for all three experiments. Error bars represent the standard deviation. Brackets denote that there were no statistically significant differences ($p < 0.05$) between the shown bar pairs.

The statistically significant difference in the content of PEG-5k and PEG-30k coated ICG-NCs within macrophages (Fig. 7) may be attributed to differences in conformation of PEG chains on the surface of nanocapsules. Due to the large surface curvature of the nanospheres compared to flat surfaces, an increase in the length of the PEG polymers will provide conformational freedom at their distal termini that interfaces with the surrounding physiological media. Hence, as the PEG's MW increases, the conformation of PEG chains alters from a brush-like structure to a mushroom-like arrangement. The protein resistivity of a PEGylated surface with either of these conformations is different. It has been reported that the brush-like conformation can reduce protein adsorption more as a result of higher entropic repulsion between proteins and the surface.[64,65] In low MW PEG, the chains on the surface are extended away from the surface and their mobility and flexibility is higher. However, in the mushroom conformation, PEG chains are more entrapped together and flexibility is reduced. In both conformations, the PEG layer can prevent penetration of large opsonins. The small opsonins can pass through a PEG-30k layer easier due to the restricted range of motion of PEG chains compared to a PEG-5k layer.[71]

The amount of ICG-NCs in macrophages also showed a correlation with the ζ-potential of the particles. Specifically, the greatest content was associated with uncoated ICG-

NCs, which had the highest positive ζ-potential ($\approx +40$ mV peak value). The content level decreased with PEG-5k- and PEG-30k-coated ICG-NCs, which had lower peak ζ-potential values of approximately $+12$ and -7 mV, respectively. Our results are consistent with reports by Li and Huang,[44] Owens and Peppas[46] and Levchenko et al.[71] that indicate reduced uptake of PEGylated liposomes and nanoparticles by macrophages. Li and Huang have reported rapid clearance of positively charged nanoparticles from vasculature with high accumulation levels in lungs and liver.[44] When liposomes were coated with PEG or neutralized (-10 mV $< \zeta$-potential < 10 mV), their uptake by RES cells was lowered and their blood circulation half-life increased.[44]

Our results are very encouraging in that they suggest PEG-coated ICG-NCs may be used as a platform to increase the circulation time of ICG within the vasculature due to reduced interaction with human macrophages. Such a platform can potentially be used for NIR imaging and phototherapy of vascular malformations, as well as tissue abnormalities when further enhanced with surface-expressed targeting moieties.

4 Conclusion

The surface of ICG-containing nanocapsules (ICG-NCs) were successfully coated with aldehyde terminated PEG via reductive amination. PEG coating decreased the ζ-potential of ICG-NCs from high positive values to less positive potentials. Increased molecular weight (MW) of PEG from 5000 to 30000 Da resulted in further reduction of the ζ-potential toward the negative values. In comparison with free ICG and uncoated ICG-NCs, coating the surface of the capsules with PEG minimized the phagocytic content of ICG-NCs for up to 360 min, as characterized by statistically significant reductions in the mean fluorescent intensity values. Coating the surface of ICG-NCs with the low MW PEG (5000 Da) reduced the phagocytic content of ICG-NCs for at least up to 60 min in comparison with the ICG-NCs coated with the high MW PEG (30000 Da). Results of this study provide useful information on the optimum MW of PEG coating to engineer ICG-NCs with minimal uptake by RES and prolonged vascular circulation time.

Acknowledgments

This study was supported in part by the Bourns College of Engineering and the Bioengineering Center at University of California, Riverside, a grant from the National Science Foundation (CBET 0935995), and U. C. Regents Faculty Development Award (V.I.V.). The electron microscopy images were obtained at the Central Facility for Advanced Microscopy and Microanalysis (CFAMM) at UCR. The flow cytometry experiments were performed at the Institute for Integrative Genome Biology (IIGB) at UCR. Bahman Anvari dedicates this manuscript to the memory of Mr. Ardeshir Farid Modjtahedi who will remain an inspiration for pursuing knowledge.

References

1. L. R. Hirsch, A. M. Gobin, A. R. Lowery, F. Tam, R. A. Drezek, N. J. Halas, and J. L. West, "Metal nanoshells," *Ann. Biomed. Eng.* **34**(1), 15–22 (2006).
2. K. Moin, O. J. McIntyre, L. M. Matrisian, and B. F. Sloane, "Fluorescent imaging of tumors," in *In Vivo Imaging of Cancer Therapy (Cancer Drug Discovery and Development)*, A. F. Shields and P. Price, Eds., pp. 281–302, Humana Press, Totowa, NJ (2007).
3. C. Sun, J. Yang, L. Li, X. Wu, Y. Liu, and S. Liu, "Advances in the study of luminescence probes for proteins," *J. Chromatogr. B Analyt. Technol. Biomed. Life Sci.* **803**(2), 173–190 (2004).
4. M. R. Hamblin and T. N. Demidova, "Mechanisms of low level light therapy," *Proc. SPIE* **6140**, 614001 (2006).
5. G. Patonay, L. Strekowski, A. Raszkiewicz, and J. S. Kim, "Near-infrared probes: design and applications," *Proc. SPIE* **6097**, 609709 (2006).
6. J. K. Jaiswal and S. M. Simon, "Potentials and pitfalls of fluorescent quantum dots for biological imaging," *Trends Cell Biol.* **14**, 497–504 (2004).
7. X. Michalet, F. Pinaud, T. D. Lacoste, M. Dahan, M. P. Bruchez, A. P. Alivisatos, and S. Weiss, "Properties of fluorescent semiconductor nanocrystals and their application to biological labeling," *Single Mol.* **2**, 261–276 (2001).
8. J. Park, A. Estrada, K. Sharp, K. Sang, J. A. Schwartz, D. K. Smith, C. Coleman, J. D. Payne, B. A. Korgel, A. K. Dunn, and J. W. Tunnell, "Two-photon-induced photoluminescence imaging of tumors using near-infrared excited gold nanoshells," *Opt. Express* **16**, 1590–1599 (2008).
9. E. I. Altınoglu, T. J. Russin, J. M. Kaiser, B. M. Barth, P. C. Eklund, M. Kester, and J. H. Adair, "Near-infrared emitting fluorophore doped calcium phosphate nanoparticles for *in vivo* imaging of human breast cancer," *ACS Nano* **2**, 2075–2084 (2008).
10. E. I. Altınoglu and J. H. Adair, "Near infrared imaging with nanoparticles," *Wiley Interdisciplinary Reviews: Nanomedicine and Nanobiotechnology* **2**(5), 461–477 (2010).
11. M. L. J. Landsman, G. Kwant, G. A. Mook, and W. G. Zijlstra, "Light-absorbing properties, stability, and spectral stabilization of indocyanine green," *J. Appl. Physiol.* **40**, 575–583 (1976).
12. R. C. Benson and H. A. Kues, "Fluorescence properties of indocyanine green as related to angiography," *Phys. Med. Biol.* **23**(1), 159–163 (1978).
13. T. Desmettre, J. M. Devoiselle, and S. Mordon, "Fluorescence properties and metabolic features of indocyanine green (ICG) as related to angiography," *Surv. Ophthalmol.* **45**(1), 15–27 (2000).
14. A. El-Desoky, A. M. Seifalian, M. Cope, D. T. Delpy, and B. R. Davidson, "Experimental study of liver dysfunction evaluated by direct indocyanine green clearance using near infrared spectroscopy," *Br. J. Surg.* **86**, 1005–1011 (1999).
15. J. G. Webster, "Measurement of flow and volume of blood" In *Medical Instrumentation: Application and Design*, G. Webster, Ed., Wiley, New York (1998).
16. C. Abels, S. Fickweiler, P. Weiderer, W. Bäumler, F. Hofstädter, M. Landthaler, and R. M. Szeimies, "Indocyanine green (ICG) and laser irradiation induce photooxidation," *Arch. Dermatol. Res.* **292**(8), 404–411 (2000).
17. P. Babilas, G. Shafirstein, J. Baier, V. Schacht, R. M. Szeimies, M. Landthaler, W. Baumler, and C. Abels, "Photothermolysis of blood vessels using indocyanine green and pulsed diode laser irradiation in the dorsal skinfold model chamber," *Lasers Surg. Med.* **39**, 341–352 (2007).
18. M. A. Yassen, P. Diagaradjane, B. M. Pikkula, J. Yu, M. S. Wong, and B. Anvari, "Photothermal and photochemical effects of laser light absorption by indocyanine green (ICG)," *Proc. SPIE* **5695**, 27–35 (2005).
19. E. A. Genina, A. N. Bashkatov, G. V. Simonenko, O. D. Odoevskaya, V. V. Tuchin, and G. B. Altshuler, "Low-intensity indocyanine-green laser phototherapy of acne vulgaris: pilot study," *J. Biomed. Opt.* **9**(4), 828–834 (2004).
20. N. K. Rho, D. K. Lee, S. Kim, D. P. Lee, and C. W. Jeong, "Efficacy of acne treatment using a combination of radiofrequency energy and indocyanine green-mediated pulsed light phototherapy," *Lasers Surg. Med.* **40**, 32 (2008).
21. K. Urbanska, B. Romnaowska-Dixon, Z. Matuszak, J. Oszajca, P. Nowak-Sliwinska, and G. Stochel, "Indocyanine green as a prospective sensitizer for photodynamic therapy of melanomas," *Acta Biochem. Pol.* **49**(2), 387–391 (2002).

22. W. W. Tseng, R. E. Saxton, A. Deganutti, and C. D. Liu, "Infrared laser activation of indocyanine green inhibits growth in human pancreatic cancer," *Pancreas* **27**(3), 42–45 (2003).
23. O. Bozkulak, R. F. Yamaci, O. Tabakoglu, and M. Gulsoy, "Toxic effects of 809-nm diode laser and indocyanine green on MDA-MB231 breast cancer cells," *Photodiagnosis Photodyn. Ther.* **6**(2), 117–121 (2009).
24. W. Baumler, C. Abels, S. Karrer, T. Wei, H. Messmann, M. Landthaler, and R. M. Szeimies, "Photooxidative killing of human colonic cancer cells using indocyanine green and infrared light," *Br. J. Cancer* **80**(3–4), 360–363 (1999).
25. M. Mauerer, A. Penzkofer, and J. Zweck, "Dimerization, J-aggregation and J-disaggregation dynamics of indocyanine green in heavy water," *J. Photochem. Photobiol., B* **47**(1), 68–73 (1998).
26. R. Philip, A. Penzkofer, W. Bäumler, R. M. Szeimies and C. Abels, "Absorption and fluorescence spectroscopic investigation of indocyanine green," *J. Photochem. Photobiol., A* **96**(1–3), 137–148 (1996).
27. V. Saxena, M. Sadoqi, and J. Shao, "Degradation kinetics of indocyanine green in aqueous solution," *J. Pharm. Sci.* **92**(10), 2090–2097 (2003).
28. K. J. Baker, "Binding of sulfobromophthalein (BSP) sodium and indocyanine green (ICG) by plasma α_1-lipoprotein," *Proc. Soc. Exp. Biol. Med.* **122**, 957–963 (1966).
29. K. Kamisaka, Y. Yatsuji, H. Yamada, and H. Kameda, "The binding of indocyanine green and other organic anions to serum proteins in liver disease," *Clin. Chim. Acta* **53**, 255–264 (1974).
30. S. G. Sakka, H. Koeck, and A. Meier-Hellmann, "Measurement of indocyanine green plasma disappearance rate by two different dosages," *Intensive Care Med.* **30**, 506–509 (2004).
31. S. G. Sakka and N. van Hout, "Relation between indocyanine green (ICG) plasma disappearance rate and ICG blood clearance in critically ill patients," *Intensive Care Med.* **32**, 766–769 (2006).
32. M. A. Yaseen, J. Yu, M. S. Wong, and B. Anvari, "Stability assessment of indocyanine green within dextran-coated mesocapsules by absorbance spectroscopy," *J. Biomed. Opt.* **12**(6), 064031 (2007).
33. V. Saxena, M. Sadoqi, and J. Shao, "Enhanced photo-stability, thermal-stability and aqueous-stability of indocyanine green in polymeric nanoparticulate systems," *J. Photochem. Photobiol., B* **74**(1), 29–38 (2004).
34. V. B. Rodriguez, S. M. Henry, A. S. Hoffman, P. S. Stayton, X. Li, and S. H. Pun, "Encapsulation and stabilization of indocyanine green within poly(styrene-alt-maleic anhydride) block-poly(styrene) micelles for near-infrared imaging," *J. Biomed. Opt.* **13**(1), 014025 (2008).
35. A. J. Gomes, L. O. Lunardi, J. M. Marchetti, C. N. Lunardi, and A. C. Tedesco, "Indocyanine green nanoparticles useful for photomedicine," *Photomed. Laser Surg.* **24**(4), 514–521 (2006).
36. T. J. Desmettre, S. Soulie-Begu, J. M. Devoisselle, and S. R. Mordon, "Diode laser-induced thermal damage evaluation on the retina with a liposome dye system," *Lasers Surg. Med.* **24**, 61–68 (1999).
37. S. Mordon, J. M. Devoisselle, S. Begu, and T. Desmettre, "Laser-induced release of liposome-encapsulated dye: a new diagnostic tool," *Lasers Med. Sci.* **13**, 181–188 (1998).
38. G. Kim, S. W. Huang, K. C. Day, M. O'Donnell, R. R. Agayan, M. A. Day, R. Kopelman, and S. Ashkenazi, "Indocyaninegreen- embedded PEBBLEs as a contrast agent for photoacoustic imaging," *J. Biomed. Opt.* **12**, 044020 (2007).
39. J. Yu, M. A. Yaseen, B. Amvari, and M. S. Wong, "Synthesis of near-infrared-absorbing nanoparticle- assembled capsules," *Chem. Mater.* **29**, 1277–1284 (2007).
40. M. A. Yaseen, J. Yu, M. S. Wong, and B. Anvari, "Laser-induced heating of dextran-coated mesocapsules containing indocyanine green," *Biotechnol. Prog.* **23**, 1431–1440 (2007).
41. M. A. Yaseen, J. Yu, M. S. Wong, and B. Anvari, "Biodistribution of encapsulated ICG in healthy mice," *Mol. Pharmacol.* **6**(5), 1321–1332 (2009).
42. M. A. Yaseen, J. Yu, M. S. Wong, and B. Anvari, "In-vivo fluorescence imaging of mammalian organs using charge-assembled msesocapsule constructs containing indocyanine green," *Opt. Express* **16**(25), 20577–20587 (2008).
43. J. Yu, D. Javier, M. A. Yaseen, N. Nitin, R. Richards-Kortum, B. Anvari, and M. S. Wong, "Self-assembly synthesis, tumor cell targeting, and photothermal capabilities of antibody-coated indocyanine green nanocapsules," *J. Am. Chem. Soc.* **132**, 1929–1938 (2010).
44. S. D. Li and L. Huang, "Pharmacokinetics and biodistribution of nanoparticles," *Mol. Pharmacol.* **5**(4), 496–504 (2008).
45. P. Opanasopit, M. Nishikawa, and M. Hashida, "Factors affecting drug and gene delivery: effects of interaction with blood components," *Crit. Rev. Ther. Drug Carrier Syst.* **19**, 191–233 (2002).
46. D. E. Owens and N. A. Peppas, "Opsonization, biodistribution, and pharmacokinetics of polymeric nanoparticles," *Int. J. Pharm.* **307**, 93–102 (2006).
47. F. Alexis, E. Pridgen, L. K. Molnar, and O. C. Farokhzad, "Factors affecting clearance and biodistribution of polymeric nanoparticles," *Mol. Pharmacol.* **5**(4), 505–515 (2008).
48. A. S. Zahr, C. A. Davis, and M. V. Pishko, "Macrophage uptake of core-shell nanoparticles surface modified with poly(ethylene glycol)," *Langmuir* **22**(19), 8178–8185 (2006).
49. L. Illum and S. S. Davis, "The organ uptake of intravenously administered colloidal particles can be altered using a non-ionic surfactant (Poloxamer 338)," *FEBS Lett.* **167**(1), 79–82 (1984).
50. L. Illum, S. S. Davis, R. H. Müller, E. Mak, and P. West, "The organ distribution and circulation time of intravenously injected colloidal carriers sterically stabilized with a blockcopolymer – poloxamine 908," *Life Sci.* **40**(4), 367–374 (1987).
51. G. Kaul and M. Amiji, "Long-circulating poly(ethylene glycol)-modified gelatin nanoparticles for intracellular delivery," *Pharm. Res.* **19**(7), 1061–1067 (2002).
52. G. Kaul and M. Amiji, "Biodistribution and targeting potential of poly(ethylene glycol)-modified gelatin nanoparticles in subcutaneous murine tumor model," *J. Drug Target.* **12**(9), 585–591 (2004).
53. R. G. Chapman, E. Ostuni, S. Takayama, R. E. Holmlin, L. Yan, and G. M. Whitesides, "Surveying for surfaces that resist the adsorption of proteins," *J. Am. Chem. Soc.* **122**, 8303–8304 (2000).
54. A. S. Hoffman, "Non-fouling surface technologies," *J. Biomater. Sci., Polym. Ed.* **10**(10), 1011–1014 (1999).
55. J. Israelachvili, "The different faces of poly(ethylene glycol)," *Proc. Natl. Acad. Sci. U.S.A.* **94**(16), 8378–8379 (1997).
56. S. I. Jeon, J. H. Lee, J. D. Andrade, and P. G. De Gennes, "Protein-surface interactions in the presence of polyethylene oxide: I. Simplified theory," *J. Colloid Interface Sci.* **142**(1), 149–158 (1991).
57. R. Gref, Y. Minamitake, M. T. Peracchia, V. Trubetskoy, V. Torchilin, and R. Langerll, "Biodegradable long-circulating polymeric nanospheres," *Science* **263**(5153), 1600–1603 (1994).
58. R. Gref, M. Luck, P. Quellec, M. Marchand, E. Dellacherie, S. Harnisch, T. Blunk, and R. H. Muller, " 'Stealth' corona-core nanoparticles surface modified by polyethylene glycol (PEG): influences of the corona (PEG chain length and surface density) and of the core composition on phagocytic uptake and plasma protein adsorption," *Colloids Surf., B* **18**, 301–313 (2000).
59. Z. Yang, J. A. Galloway, and H. Yu, "Protein interactions with poly(ethylene glycol) self-assembled monolayers on glass substrates: diffusion and adsorption," *Langmuir* **15**, 8405–8411 (1999).
60. A. Roosjen, H. C. Van Der Mei, H. J. Busscher, and W. Norde, "Microbial adhesion to poly(ethylene oxide) brushes: influence of polymer chain length and temperature," *Langmuir* **20**(25), 10949–10955 (2004).
61. J. Wan, M. S. Thomas, S. Guthrie, and V. I. Vullev, "Surface-bound proteins with preserved functionality," *Ann. Biomed. Eng.* **37**(6), 1190–1205 (2009).
62. V. Zoulalian, S. Zurcher, S. Tosatti, M. Textor, S. Monge, and J. J. Robin, "Self-assembly of poly(ethylene glycol)-poly(alkyl phosphonate) terpolymers on titanium oxide surfaces: synthesis, interface characterization, investigation of nonfouling properties, and long-term stability," *Langmuir* **26**(1), 74–82 (2009).
63. M. Pantusa, L. Sportelli, and R. Bartucci, "Spectroscopic and calorimetric studies on the interaction of human serum albumin with DPPC/PEG: 2000-DPPE membranes," *Eur. Biophys. J.* **37**, 961–973 (2008).
64. Z. Xu, N. B. Holland, and R. E. Marchant, "Conformations of short-chain poly(ethylene oxide) lipopolymers at the air-water interface: a combined film balance and surface tension study," *Langmuir* **17**, 377–383 (2001).

65. P. Harder, M. Grunze, R. Dahint, G. M. Whitesides, and P. E. Laibinis, "Molecular conformation in oligo(ethylene glycol)-terminated self-assembled monolayers on gold and silver surfaces determines their ability to resist protein adsorption," *J. Phys. Chem. B* **102**, 426–436 (1998).
66. E. W. Baxter and A. B. Reitz, "Reductive aminations of carbonyl compounds with borohydride and borane reducing agents," in *Organic Reactions*, L. E. Overman, Ed., pp. 4–7, John Wiley & Sons, Inc., New York (2004).
67. V. Saxena, M. Sadoqi, J. Shao, and S. Kumar, "Enhanced intracellular uptake of indocyanine green by oolymeric nanoparticulate delivery systems," *J. Biomed. Nanotech.* **1**(2), 168–175 (2005).
68. S. M. Moghimia and J. Szebeni, "Stealth liposomes and long circulating nanoparticles: critical issues in pharmacokinetics, opsonization and protein-binding properties," *Prog. Lipid Res.* **42**, 463–478 (2003).
69. Q. He, J. Zhang, J. Shi, Z. Zhu, L. Zhang, W. Bu, L. Guo, and Y. Chen, "The effect of PEGylation of mesoporous silica nanoparticles on nonspecific binding of serum proteins and cellular responses," *Biomaterials* **31**, 1085–1092 (2010).
70. K. Emoto, Y. Nagasaki, M. Iijima, M. Kato, and K. Kataoka, "Preparation of non-fouling surface through the coating with core-polymerized block copolymer micelles having aldehyde-ended PEG shell," *Colloids Surf., B* **18**, 337–346 (2000).
71. T. S. Levchenko, R. Rammohan, A. N. Lukyanov, K. R. Whiteman, and V. P. Torchilin, "Liposome clearance in mice: the effect of a separate and combined presence of surface charge and polymer coating," *Int. J. Pharm.* **240**, 95–102 (2002).